SPACEBORNE SAR ANATOMY OF A CITY

Daniele Perissin [(1)], Alessandro Ferretti [(2)], Claudio Prati [(1)]

[(1)] Politecnico di Milano
Piazza L. da Vinci 32, 20133 Milano, Italy
Email: perissin@elet.polimi.it
[(2)] Tele-Rilevamento Europa T.R.E.
Via V. Colonna 7, 20149 Milano, Italy
Email: alessandro.ferretti@treuropa.com

ABSTRACT

The ensemble of stable radar targets (the so-called Permanent Scatterers -PS-, [1], [2]) in urban area can be interpreted as the radar skeleton of a city. By means of the PS technique, developed at POLIMI, the skeleton radar reflectors are exploited for overcoming the difficulties related to the conventional SAR interferometry approach (phase decorrelation and atmospheric effects), achieving millimetre accuracy in monitoring possible relative displacements. Even if the PS technique is an operational tool since 2000, the physical nature of the targets is still a subject of investigation. In this work we present the last results of this research program obtained by using 120 ERS and Envisat repeated acquisitions on the area of Milano (Italy). First, the PS's position and their elevation with respect to the ground are estimated with high precision. Then the scattering pattern of targets as a function of their geometrical characteristics (dimensions and orientation) is analysed. The variation of the Radar Cross Section as a function of the acquisition geometry (normal baseline and Doppler centroid) is linked to the extension of the scatterer in range and azimuth. Temperature dependent amplitude variations have been exploited for individuating retro-reflecting periodic structures (Bragg scattering). Exploiting the auto-interferogram generated from an Envisat Alternating Polarization acquisition, odd and even bounces of radar echoes are identified thus separating dihedrals from specular or trihedral reflectors [8]. Finally, by means of the collected radar measurements, 5 principal PS typologies have been identified: ground retro-reflectors (gratings), elevated retro-reflectors (roofs), dihedrals, poles and trihedrals.

1 INTRODUCTION

The Permanent Scatterers (PS) technique is a powerful operational tool for monitoring ground deformations on a large number of natural coherent targets (up to 100 PS/Km^2 in urban areas), exploiting long series of SAR data [1], [2]. The most attractive aspect of this approach is the capability of providing measurements relative to individual radar targets with unprecedented precision. Even if the PS technique has been used since the late nineties, the physical nature of PS's is still under investigation as a key step for a correct interpretation of the measured deformation mechanism. As an example, the phase of a dihedral formed by the ground and a building wall does not change in presence of buildings slow subsidence, but it changes in case of ground subsidence [7]. In second instance, the classification of reflecting structures behaving as PS allows an a-priori identification of the PS's looking at the structural details of buildings. Finally, if we know the PS's physical nature, we can foresee their electromagnetic behaviour under different acquisition geometries, frequencies and polarizations, and we can develop feasibility studies on the integration of interferometric SAR multiple sensors (e.g. ERS and Envisat coherent exploitation [5], [6] or the future Radarsat 1 and Radarsat 2 coherent exploitation). In this paper we describe the methodology adopted to tackle the problem of the PS physical nature and we report the principal results we obtained.

2 PHYSICAL ANALYSIS

The present work is based on the analysis of 120 SAR images of town of Milano where ground truth data are easily accessible to us. The 120 SAR images dataset has been acquired by ERS-1, ERS-2 and Envisat satellites from 1992 to 2005. Normal baseline values range from –4000*m* to 4000*m* and Doppler Centroid from -4 to 4 PRF (such a wide DC range is mainly due to ERS-2 acquisitions in gyro-less mode). Moreover, two 16*MHz* spectral bands centred around 5.3*GHz* (ERS radar frequency) and 5.331*GHz* (Envisat radar frequency) have been exploited. The processed area covers 16x18Km^2 around the city-centre. About 60,000 PS's have been detected with coherence $\gamma>0.7$. Three main measurements have been carried out for each PS: the elevation with respect to the ground, the radiation pattern and the auto-interferogram phase of an Envisat alternating polarization acquisition.

2.1 Elevation

The PS location should be known within a few meters accuracy in the 3D space to be able to associate the PS to a physical structure. To this aim we exploit the PS relative height that, together with the deformation rate, is the principal product of the PS analysis. The PS approach is described in detail in [1], [2] and PS positioning results are reported in [3]. Here, we wish briefly recall that, for a given PS with slant range position and elevation respectively Δr and Δq (relative to the centre of the sampling cell), the following expression of the geometric component of the interferometric phase holds:

$$\Delta\phi = \frac{4\pi}{\lambda}\left(\Delta r \frac{B_n}{R_M \tan\theta} + \Delta q \frac{B_n}{R_M \sin\theta}\right) \tag{1}$$

Here λ is the radar wavelength, B_n the normal baseline, R_M the sensor-target distance and θ the incidence angle. The first term is related to the flat terrain and can be compensated exploiting the WGS84 ellipsoid and the satellite state vectors. The second term contains the target height, which can be estimated as the value that fits the measurement. In Figure 1 we report the PS's ellipsoidal elevation so found along the North (Gauss-Boaga) coordinate after removal of the low-pass topography [3]. In this way the PS elevation has been referred to the surrounding ground level. In Figure 1, focusing the attention on details, one can appreciate some set of adjacent points with high elevations, describing high regular structures (as the San Siro stadium and the central station). It is worth also noting the thickening of high points around the centre of Milan, where the buildings are higher and closer among themselves. We wish to point out that such a precision of PS height estimate is due to the high dispersion of normal baseline values, ranging from –4000*m* to 4000*m*. With such a dataset, despite of the presence of a few outliers, the achieved average elevation accuracy is close to 1*m* [3].

2.2 Radiation pattern

The identification of each PS backscattering pattern as a function of the acquisition parameters is the second step of the PS's characterization. It should be pointed out that ERS-2 loss of gyroscopes, usually seen as a negative fact, turns out to be a very positive circumstance to get the scatterer microwave radiation pattern. The PS backscattering radiation pattern has been modelled with two cardinal sines as a function of normal baseline and Doppler centroid (DC). Each cardinal sine is characterized by two parameters: width and orientation. As far as range is concerned, the PS backscattering radiation pattern observed by the satellite as a function of the normal baseline B_n is a cardinal sine whose main lobe width is inversely proportional to the target extension L_x measured along the normal to the slant range. The main lobe position B_{n0} on the normal baseline axis indicates the target pointing.

$$s(B_n) = \mathrm{sinc}\left[\frac{2L_x}{\lambda R_M}(B_n - B_{n0})\right] \tag{2}$$

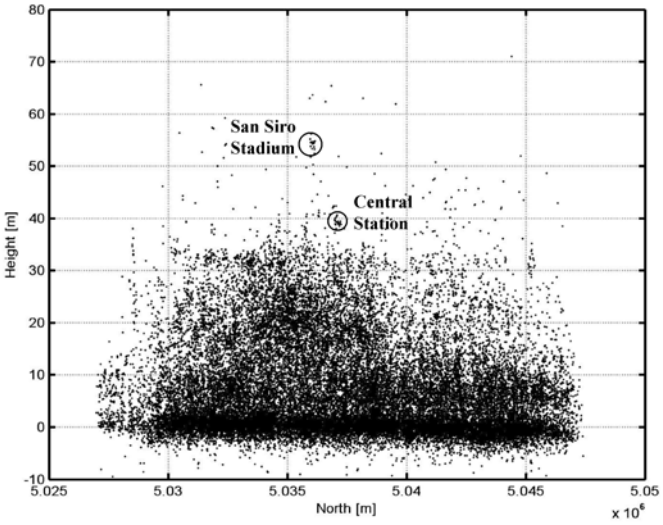

Fig. 1. PS elevation with respect to the ground as a function of the North coordinate (Gauss-Boaga) in Milan [3].

Likewise we obtain for the azimuth dimension a backscattering radiation pattern as a function of the DC variation with respect to the master image Δf_{DC} :

$$s(\Delta f_{DC}) = \mathrm{sinc}\left[\frac{L_{az}}{PRF\,\delta_{az}} (\Delta f_{DC} - \Delta f_{DC0}) \right] \tag{3}$$

Here PRF is the pulse repetition frequency and δ_{az} the azimuth sampling step.
In order to correctly analyse the target radiation pattern, also a possible limited life-time has to be taken into account [4]. The amplitude behaviour of a target with a life cycle shorter than the dataset time-span can be simply described with a rectangular function between born and death dates t_{on} and t_{off}:

$$s(t) = rect_{t_{on}, t_{off}}(t) \tag{4}$$

Finally we consider the effects of the thermal conditions on the target radar response. In fact, the dilation caused by a temperature change can modify the pointing of a periodic structure resonating toward the sensor (the pointing of a Bragg scattering target depends on the distance between the reflecting elements). Consequently, the amplitude of the radar signal can vary with the temperature at the acquisition time. Such an effect can be compared to that caused by a view-angle change. It can be shown that for a horizontal metal retro-reflecting structure 30°C of temperature are equivalent to about 300*m* of normal baseline. Due to the limited values range, the amplitude as a function of the temperature change ΔT has been linearized, obtaining

$$s(\Delta T) = s_0 (1 - k_T \Delta T) \tag{5}$$

In Eq. 5 k_T [°C^{-1}] is the amplitude-temperature constant, and it can be used for identifying resonating structures.
Figure 2 shows some of the estimated parameters of the PS back-scattering pattern in the Milan dataset. The two images in the upper part of figure 2 show the histograms of PS's range and azimuth width obtained by means of the sinc model. The peaks on zero width identify the targets with flat scattering pattern (like trihedrals or dihedrals). The two images in the lower part of figure 2 are born and death dates of the detected PS's. About 20% of PS's have a life cycle shorter than the data-set time-span.

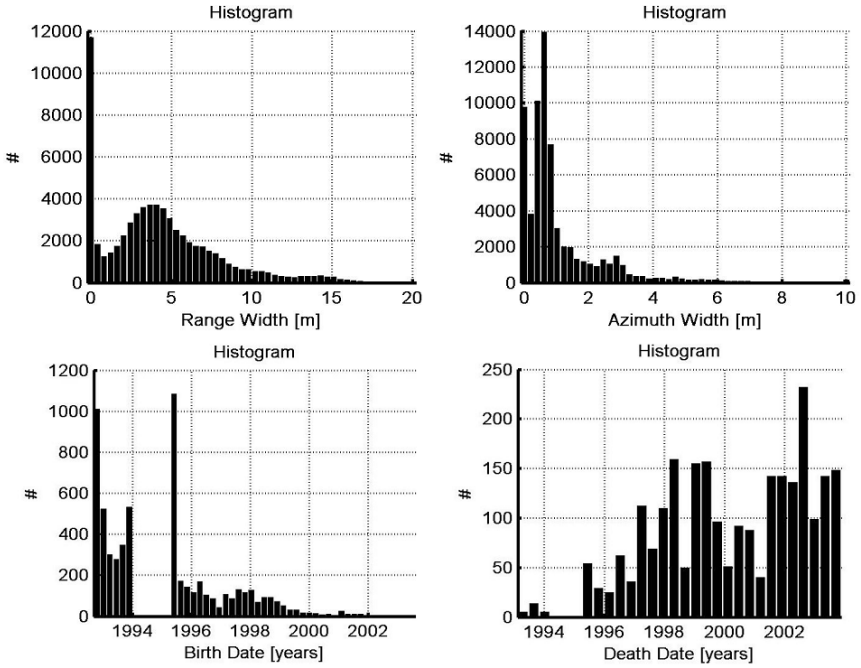

Fig. 2. Histograms of 4 scattering pattern parameters of the PS's in Milan. Up left: range width. Up right: azimuth width. Down left: born date. Down right: death date.

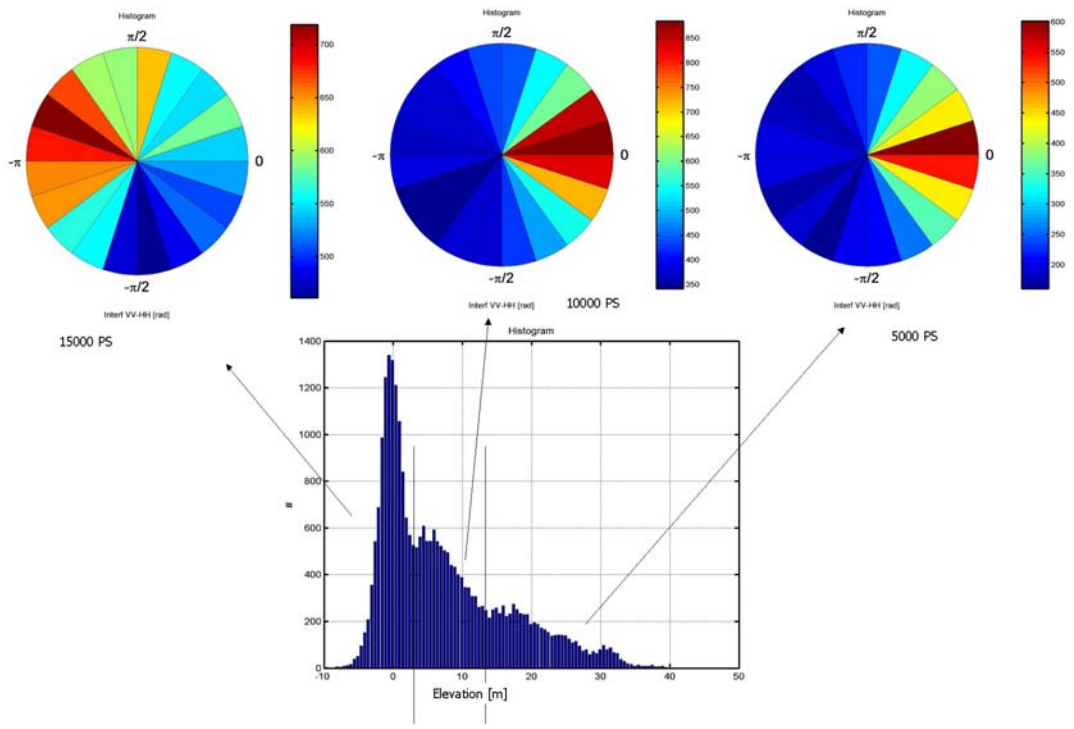

Fig. 3. AP auto-interferogram phase [rad] histograms for different elevation classes. Below: PS's elevation [m] histogram. On the ground double bounces dominate, while at higher elevations most are even.

2.3 Alternating polarization

In the alternating polarization acquisition mode, Envisat takes simultaneously 2 images with 2 different polarizations of the same area, with the same acquisition geometry but with half azimuth resolution. Creating an interferogram between the two images (auto-interferogram), in correspondence "good" scatterers (where the 2 different spectra are coherent) the interferometric phase depends only on the polarimetric response of the scatterers [8]. Thus the polarimetric auto-interferogram can be exploited for discerning between odd and even bounces. A specular reflector (a mirror) behaves in the same way if illuminated with horizontal or vertical polarised signals (0 auto-interferometric phase), whereas a dihedral rotates the phase by π radians [8], [9].
In Figure 3 three histograms of the auto-interferometric phase are shown for different elevation classes of the PS's in Milan. It's interesting to observe that the probability to have dihedrals at ground level is quite high, while at higher elevations odd-bounces dominate (tiled roofs or corrugated iron roofs are good back-scatterers).

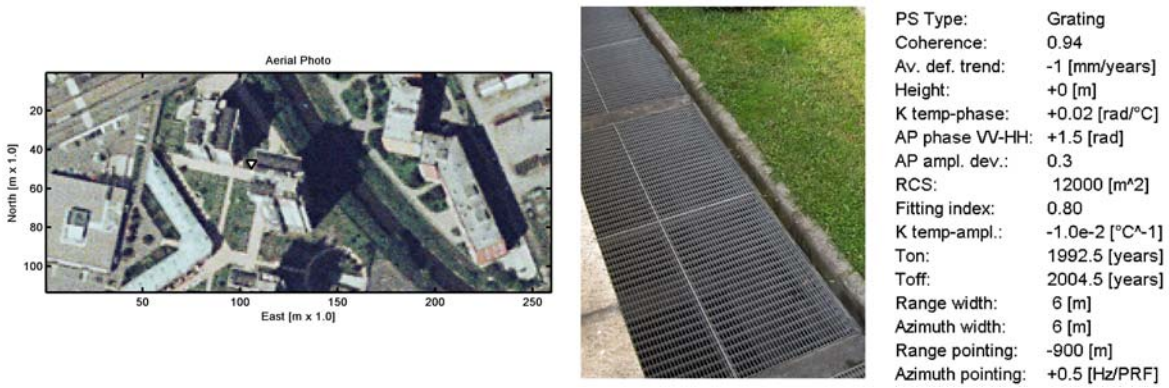

Fig. 4. PS example in Milan: floor metal grating. Left: aerial photo and PS position. Centre: target photo. Right: list of the PS estimated parameters (height h=0m, width L_x=6m L_y=6m, temperature-dependency k_T=-.01°C^{-1}).

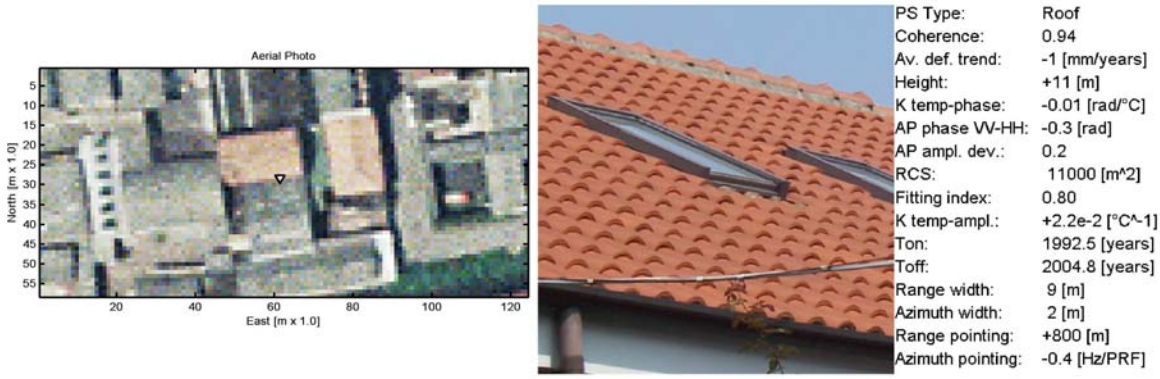

Fig. 5. PS example in Milan: tiled roof. Left: aerial photo and PS position. Centre: target photo. Right: list of the PS estimated parameters (height h=11m, width L_x=9m L_y=2m, temperature-dependency k_T=-.02°C^{-1}).

2.4 Target typologies

The described radar measurements can be jointly exploited for identifying and characterizing urban SAR PS's. Thus we discovered that the principal urban target typologies are the following:

- Back-scattering floor gratings -periodical ground metal structures- (low elevation, wide in range, wide in azimuth, middle RCS, AP phase 0), see Figure 4. Generally not visible under different geometries.
- Back-scattering roofs -periodical elevated structures- (high elevation, wide in range, wide in azimuth, middle-low RCS, AP phase 0), see Figure 5. Generally not visible under different geometries.
- Dihedrals formed by wall and ground (low elevation, narrow in range, wide in azimuth, high RCS, AP phase π), see Figure 6. This kind of targets is visible from different parallel tracks.
- Dihedrals with circular symmetry like poles (low elevation, narrow in range, narrow in azimuth, low RCS, AP phase π), see Figure 7. These are targets that can be seen from ascending and descending passes.
- Trihedrals corresponding to internal angles of courtyards (low elevation, narrow in range, narrow in azimuth, high RCS, AP phase 0), see Figure 8. Visible from different parallel tracks.

3 CONCLUSIONS

The results on the PS physical nature show that:

- PS's position can be measured with an accuracy of about 1m only if large baselines and Doppler centroids are exploited.
- PS's backscattering radiation pattern and thus their dimension and pointing angle can be roughly estimated by exploiting very large baselines and Doppler centroids.
- Dihedrals can be discriminated from specular or trihedrals reflectors by exploiting AP acquisitions
- Urban SAR PS's typologies, recognizable by means of radar measurements, are dihedrals, poles, trihedrals, floor gratings, roofs.
- Urban SAR PS characterization allows the identifications of targets visible by different sensors.

Fig. 6. PS example in Milan: dihedral in a park. Left: aerial photo and PS position. Centre: target photo. Right: list of the PS estimated parameters (height h=0m, point-wise in range L_x=0m, AP phase –2.4rad).

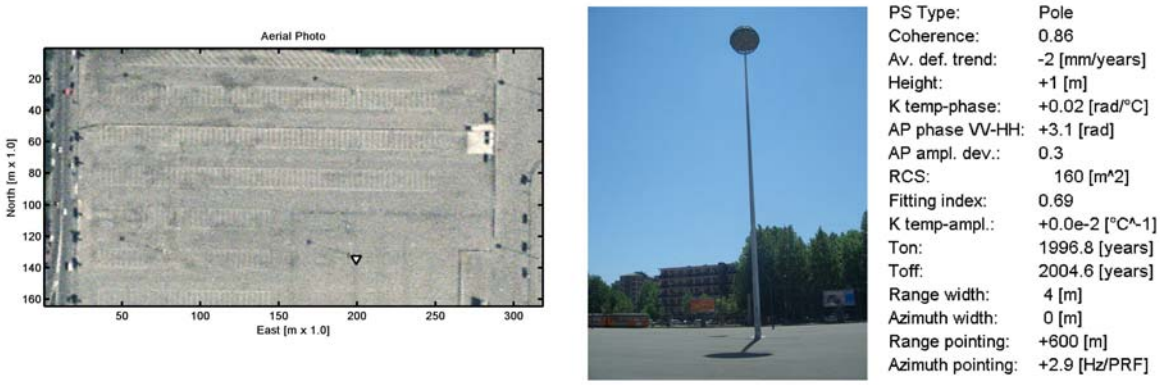

Fig. 7. PS example in Milan: pole on a car park. Left: aerial photo and PS position. Centre: target photo. Right: list of the PS estimated parameters (height h=0m, low RCS, small L_x=4m L_y=0m, AP phase 3.1rad).

References

1. Ferretti A., Prati C., Rocca F., Permanent Scatterers in SAR Interferometry, IEEE TGARS, Vol. 39, no. 1, 2001.
2. Ferretti A., Prati C., Rocca F., Non-linear subsidence rate estimation using permanent scatterers in Differential SAR Interferometry, IEEE TGARS, Vol. 38, no. 5, 2000.
3. Perissin D., Rocca F., "Urban DEM", Proceedings of FRINGE 2005, Frascati (Italy), 28 November - 2 December 2005
4. Ferretti A., Colesanti C., Perissin D., Prati C., and Rocca F., Evaluating the effect of the observation time on the distribution of SAR Permanent Scatterers, Proceedings of FRINGE03, Frascati (Italy), December 2003.
5. Colesanti C., Ferretti A., Perissin D., Prati C., Rocca F., ERS-ENVISAT permanent scatterers interferometry, Geoscience and Remote Sensing Symposium, Proceedings. 2003 IEEE International , Volume: 2 , Pages:1130 - 1132 vol.2, 2003.
6. Ferretti A., Perissin D., Prati C., Rocca F., ERS-ENVISAT Permanent Scatterers Geoscience and Remote Sensing Symposium IGARSS 2004, Proceedings Anchorage (Alaska), 2004.
7. Ketelaar V.B.H., Hanssen R.F., Separation of different deformation regimes using PS-INSAR data, Proceedings of FRINGE 2003, Frascati (Italy), 1-5 December 2003
8. Inglada J., Henry C., Souyris J-C., Assessment of ASAR/IMS Multi-polarization Images Phase Difference in the Framework of Persistent Scatterers Interferometry, ENVISAT congress, Salzburg (Austria) 20-24 September 2004.
9. Van Zyl PJ., Unsupervised Classification of Scattering Behaviour using RADAR Polarimetry data, IEEE Transactions on GRS, January 1989, pp 36-45.

Fig. 8. PS example in Milan: trihedral in a court-yard. Left: aerial photo and PS position. Centre: target photo. Right: list of the PS estimated parameters (height h=2m, high RCS, small L_x=3m L_y=0m, AP phase –0.7rad).